CDS Supplementary material for LHCb-PAPER-2021-005

This appendix contains supplementary material that will be posted on the public CDS record but will not appear in the paper.

Figure 4 shows the invariant mass distribution of the $K^-K^+\pi^-$ and $\pi^-\pi^+\pi^-$ D_s^- meson final states. The candidates are selected applying the BDT requirement (orange area) and additionally passing (red circles) or failing (black squares) the particle identification (PID) requirements on the 3-tracks from the D_s^- decay. At this stage neither the PID requirement on the companion track nor the dedicated specific background vetoes are applied. The $D_s^- \to K^-K^+\pi^-$ mode is split into three samples that distinguish between resonant $D_s^- \to \phi\pi^-$ and $D_s^- \to K^{*0}K^-$ decays, and remaining non-resonant D_s^- final states. Candidates in which the K^-K^+ pair falls within $20\,\mathrm{MeV}/c^2$ of the $\phi(1020)$ mass are identified as $D_s^- \to \phi\pi^-$ decays. This requirement suppresses most of the misidentified and combinatorial background and only loose PID requirements are needed. Candidates within a $50\,\mathrm{MeV}/c^2$ window around the K^{*0} mass are identified as a $D_s^- \to K^{*0}K^-$ decays; it is kinematically impossible for a candidate to satisfy both this and the ϕ requirement. The remaining candidates are referred to as nonresonant $K^-K^+\pi^\pm$ decays. Stricter PID requirements are applied to the tracks in this sample to suppress cross-feed background. Strict PID requirements are also applied to $\pi^+\pi^-\pi^\pm$ sample. Figure 5 presents the result of the fit to the $B_s^0 \to D_s^-\pi^+$ candidates split by the D_s^- decay mode but combining magnet polarities and years of data taking.

The estimated mistag rate η, used in the decay-time fit, does not necessarily match the true mistag rate ω of the data sample and is therefore calibrated. Each tagger tag = OS, SS is calibrated independently per data sample y = 2015–2016, 2017, 2018 (2015 and 2016 data are merged due to the small integrated luminosity collected in 2015). Functions of the form

$$\omega(\eta) = \sum_{i=0}^{1} \left(f_i^{\mathrm{tag},y} + \frac{1}{2}\Delta f_i^{\mathrm{tag},y} \right) \cdot \left(\eta - \langle\eta\rangle\right)^i \,, \qquad \text{for } B_s^0$$

$$\text{and} \qquad \overline{\omega}(\eta) = \sum_{i=0}^{1} \left(f_i^{\mathrm{tag},y} - \frac{1}{2}\Delta f_i^{\mathrm{tag},y} \right) \cdot \left(\eta - \langle\eta\rangle\right)^i \,, \qquad \text{for } \overline{B}_s^0$$

are used, with the average mistag $\langle\eta\rangle^{\mathrm{tag},y}$, and the parameters $\Delta f_i^{\mathrm{tag},y}$, allowing for different calibrations for B_s^0 and $\overline{B}_s^0$ candidates. If the tagging calibration were equal for B_s^0 and $\overline{B}_s^0$ candidates, then the calibration parametrisation simplifies to $f_0 + f_1 \times (\eta - \langle\eta\rangle)$, where f_0 quantifies the measured ω for $\eta = \langle\eta\rangle$ and f_1 parametrizes the scale factor. Figure 6 shows the parameters $f_i^{\mathrm{tag},y}$ of the linear calibration of the mistag estimates η used in the decay-time fit. The fitted calibration functions are shown in Fig. 7 as orange lines with 1σ and 2σ uncertainty bands. The true mistag ω is shown in percentiles of the uncalibrated mistag η, for which the distribution is shown as a blue histogram. The combined tagging power is shown in Tab. 2.

The decay-time uncertainty estimated by the vertex fit, δ_t, is a per-candidate observable in the decay-time fit. The decay-time resolution appearing in the decay-time fit is given by

$$\sigma_t = p_0 + p_1 \cdot \delta_t \,, \tag{3}$$

where p_0 is an offset and p_1 corresponds to a scale factor. The coefficients are calibrated using the prompt $D_s^-\pi^+$ data sample. Figure 8 shows the decay-time resolution calibration (pink area). The decay-time uncertainty distribution of the $B_s^0 \to D_s^-\pi^+$ candidates is shown as the grey histogram. Similarly to the flavour tagging, the calibration parameters are determined separately for each 2015–2016, 2017, 2018 sample. Their comparison is presented in Fig. 9.

Figure 10 presents the decay-time acceptance obtained from the full Run 2 sample, assuming that before acceptance the untagged data are described by a decay-time distribution consisting of two exponentials with fixed Γ_s and $\Delta\Gamma_s$. Cubic spline functions are used to describe the acceptance for each sample separately.

A bias on the decay-time distribution of prompt $D_s^-\pi^+$ candidates is observed in data. Lower values of the total D_s^- momentum and opening angle of the bachelor π^+ tracks in the prompt sample result in larger biases on the reconstructed decay-time with respect to the signal sample. The bias measured in the prompt $D_s^-\pi^+$ data sample is calibrated using simulation before applying it to the signal $B_s^0 \to D_s^-\pi^+$ sample. Various misagligments of the tracking detector that surrounds the pp interaction have been considered and, given the precision on the detector alignment, translations in x are shown to give the largest decay-time biases. Figure 11 shows the decay-time bias, μ_t, in simulated prompt and signal samples, misaligned by a translation in x of the tracking detector, ΔT_x, between 0 and 9 µm. The pink curve is the fit used to translate the bias from the prompt to the signal data samples. Three sets of calibrated average biases in data (colored points) are shown on the plot for the same calibration curve, corresponding to different data sets used in the final decay-time fit. An illustration of the impact of decay-time bias coming from the misalignment of the VELO detector is presented in Fig. 12. The value of Δm_s is a function of the decay-time bias $\langle\mu_t\rangle_{B_s^0\to D_s^-\pi^+}$. The left plot has no correction applied on the reconstructed lifetimes and shows an increasing value of Δm_s with the bias. The right plot shows that by applying an average correction set to the size of the bias on the reconstructed decay times the fitted value of Δm_s is constant for different misalignment values. The observed decay time bias leads to a correction to Δm_s of about $0.016\,\text{ps}^{-1}$ Figure 13 shows the decay-time fit in linear and logarithmic scale combining all tagged and untagged $B_s^0 \to D_s^-\pi^+$ candidates. The blue line corresponds to the nominal fit.

Table 2: Estimated tagging power based on the calibration parameters obtained from the decay-time fit. The first uncertainty is statistical, the second obtained from the calibration procedure.

Data sample	Tagging power [%]
2015–2016	$6.03 \pm 0.03 \pm 0.27$
2017	$5.94 \pm 0.03 \pm 0.27$
2018	$6.53 \pm 0.03 \pm 0.26$
2015–2018	$6.10 \pm 0.02 \pm 0.15$

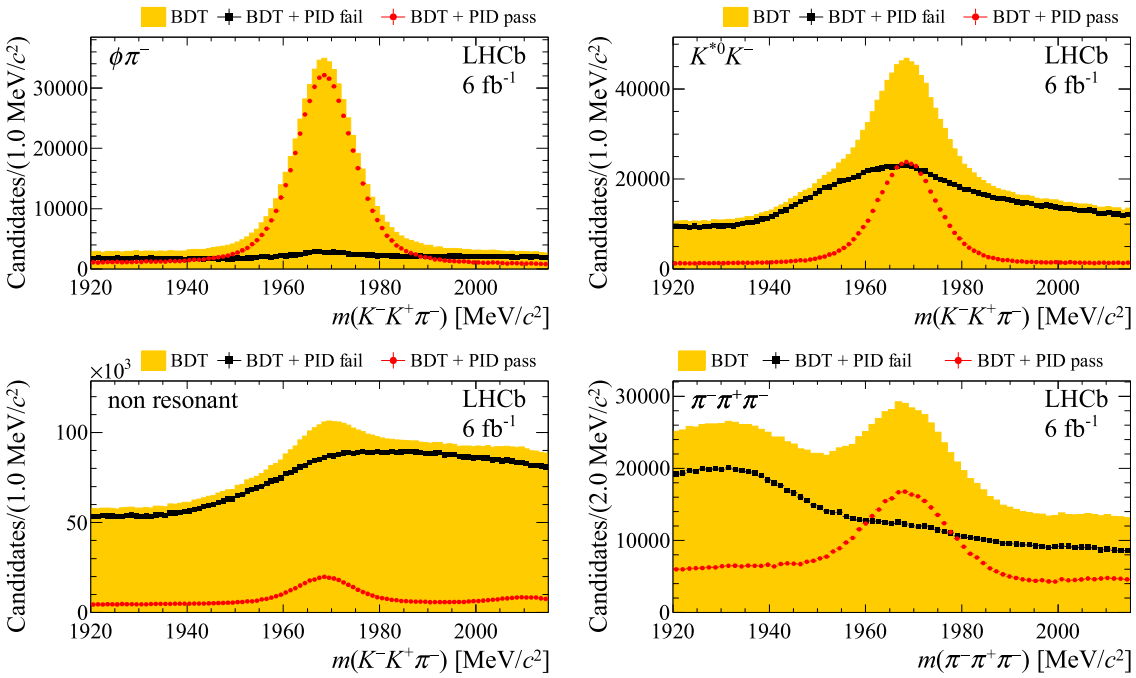

Figure 4: The D_s^- invariant mass, $m(h^-h^+h^\pm)$, distribution after the BDT selection (orange) and for candidates passing (red circles) or failing (black squares) the PID selection on the D_s^- children. There is no PID cut applied on the companion π^+ particle. $D_s^- \to \phi\pi^-$, top left, $D_s^- \to K^{*0}K^-$, top right, $D_s^- \to (K^-K^+\pi^-)_{\text{non resonant}}$, bottom left, and $D_s^- \to \pi^-\pi^+\pi^-$, bottom right, these subsamples are defined by the invariant mass cuts on the KK and $K\pi$ systems given in the text. The different level of background affecting each of these modes before and after the PID selection is clearly visible.

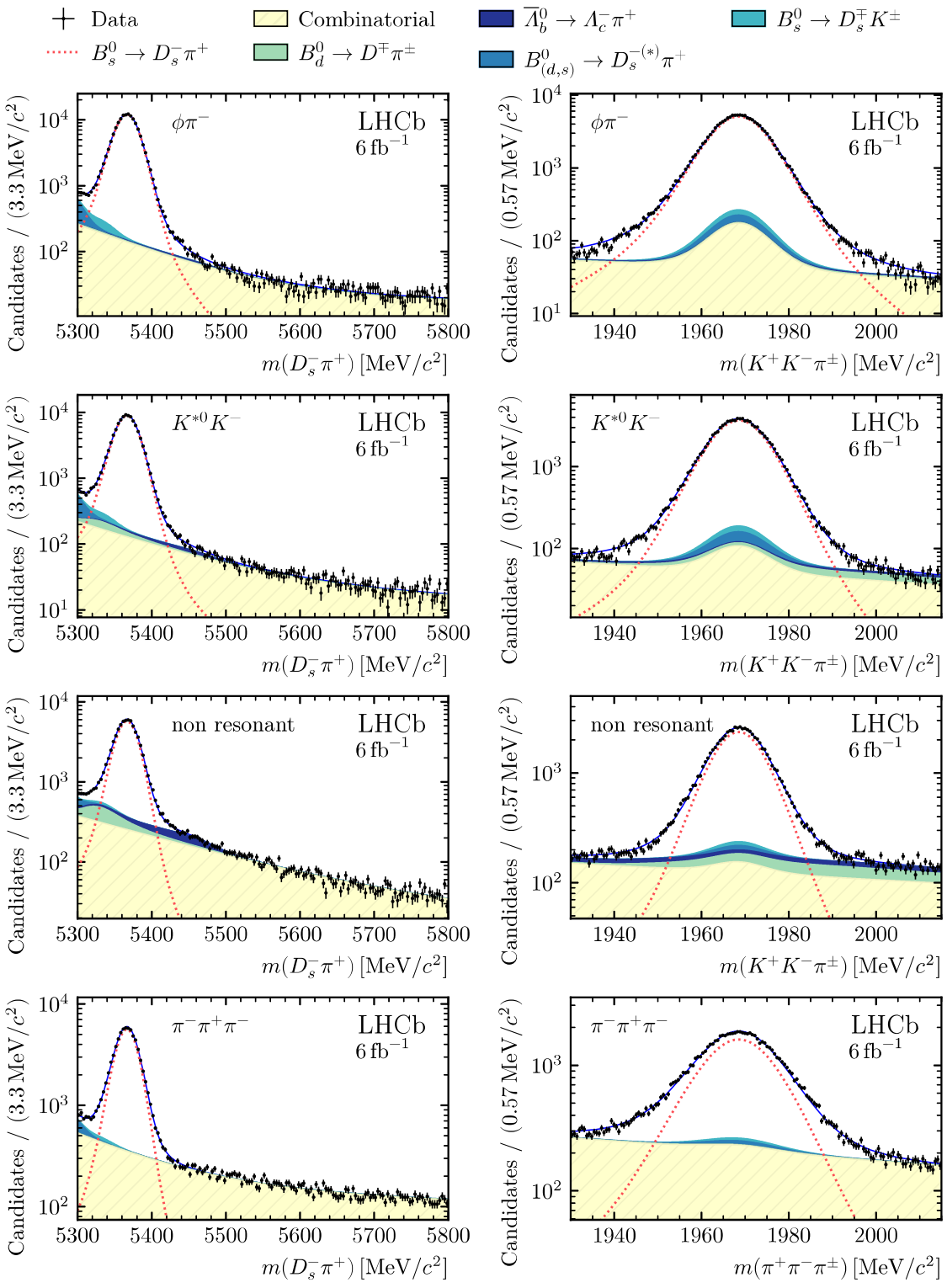

Figure 5: Result of the simultaneous fit to the $B_s^0 \to D_s^- \pi^+$ candidates. Distributions of the B_s^0, $m(D_s^-\pi^+)$, (left) and D_s^-, $m(h^-h^+h^\pm)$, (right) invariant masses for different D_s^- final states with combined magnet polarities and years of data taking with from top to bottom: $D_s^- \to \phi\pi^-$, $D_s^- \to K^{*0}K^-$, $D_s^- \to (K^-K^+\pi^-)_{\text{non resonant}}$, and $D_s^- \to \pi^-\pi^+\pi^-$. Different contributions to the fit are shown as coloured areas (for background) or dashed line (for signal).

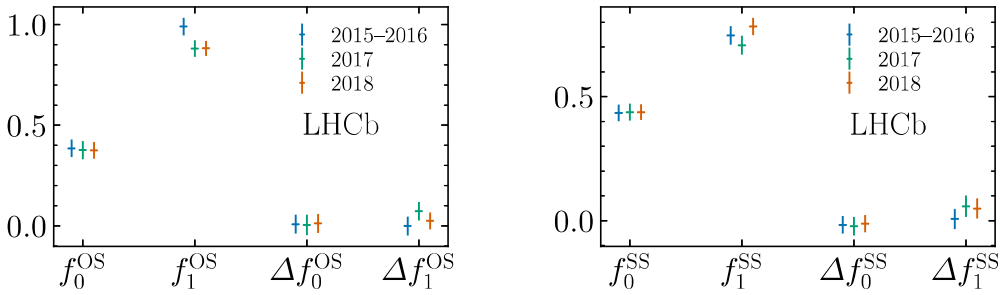

Figure 6: Calibration parameters for the OS combination (left) and the SS kaon taggers (right), obtained from the decay-time fit. Uncertainties shown are statistical only. The uncertainties of the parameters f_0 and Δf_0 are scaled by a factor 10.

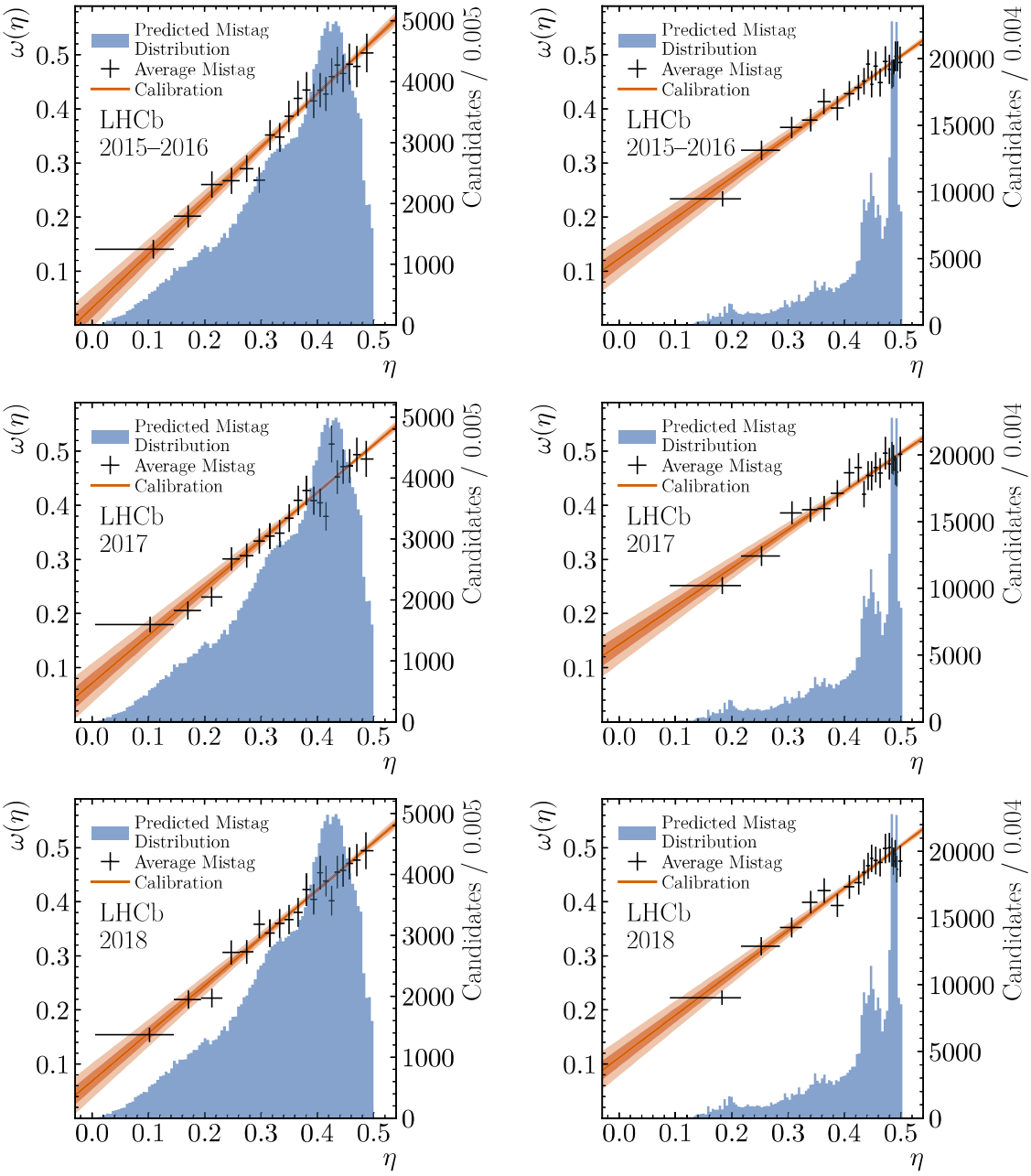

Figure 7: Distribution of (black points) mistag fractions $\omega(\eta)$ in bins of the predicted mistag η for (left) the combined OS taggers and (right) the SS Kaon tagger in the (top) 2015–2016, (middle) 2017 and (bottom) 2018 data samples. The histogram shows the distribution of η in the sample. A linear function (orange area) is used to calibrate the predicted mistag in the final decay-time fit.

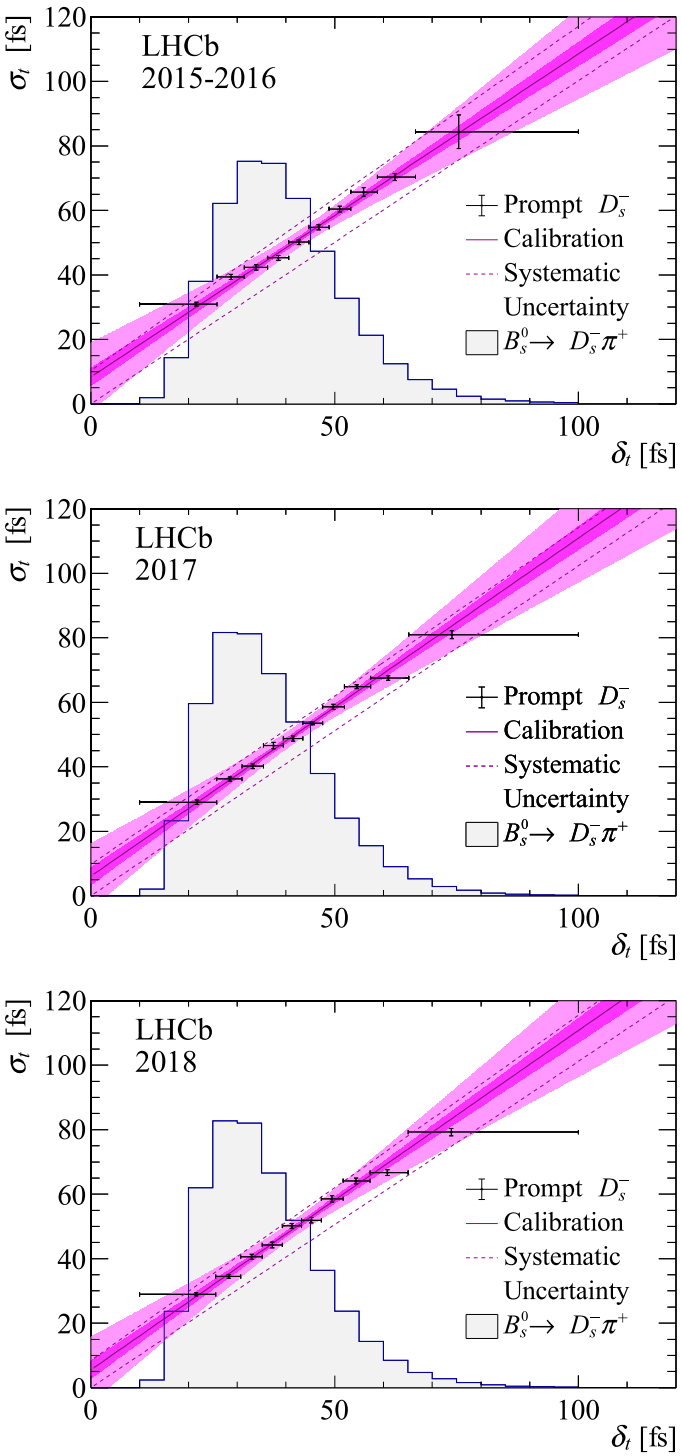

Figure 8: Decay-time resolution of prompt $D_s^- \pi^+$ candidates versus the decay-time uncertainty from the vertex fit shown for the 2015–2016, 2017 and 2018 samples. The curve indicates the result of the calibration fit. The shaded pink area gives the uncertainty on the calibration. The decay-time uncertainty distribution of the $B_s^0 \to D_s^- \pi^+$ candidates is shown as the grey histogram.

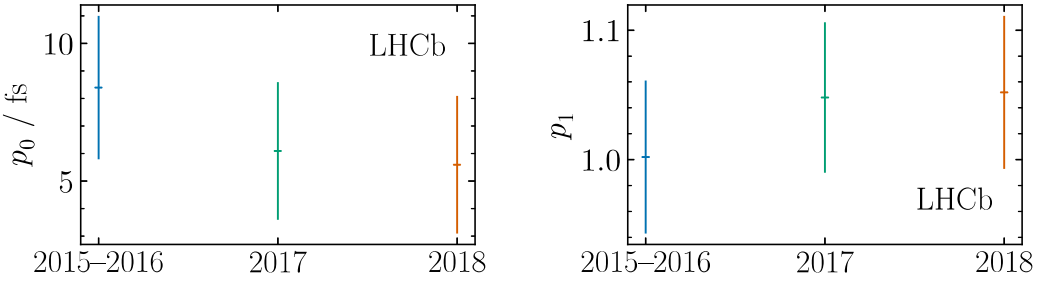

Figure 9: Decay-time resolution calibration parameters p_0 (left) and p_1 (right) used in the Δm_s fit, obtained by combining the two Gaussian widths forming the core of the prompt $D_s^-\pi^+$ decay-time distribution.

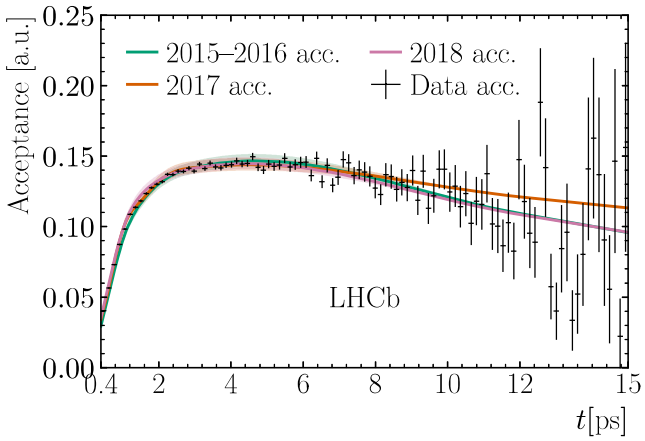

Figure 10: Decay-time acceptance obtained from the full dataset assuming an exponential distribution after acceptance correction (data points) and from cubic spline functions describing the acceptance for each dataset separately. The shaded areas indicate the 68% uncertainty intervals.

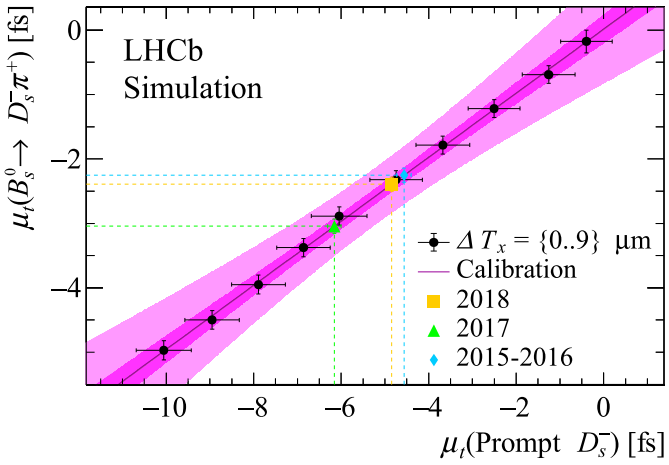

Figure 11: Decay-time bias μ_t in prompt (x axis) and signal (y axis) MC samples, misaligned by a translation, T_x, in x of the tracking detector surrounding the pp interaction region, between 0 and 9 µm. The pink curve is the calibration used to translate the bias from the prompt to the signal data samples. Three sets of calibrated average biases in data (colored points) are shown on the plot for the same calibration curve, corresponding to different data sets used in the final decay-time fit.

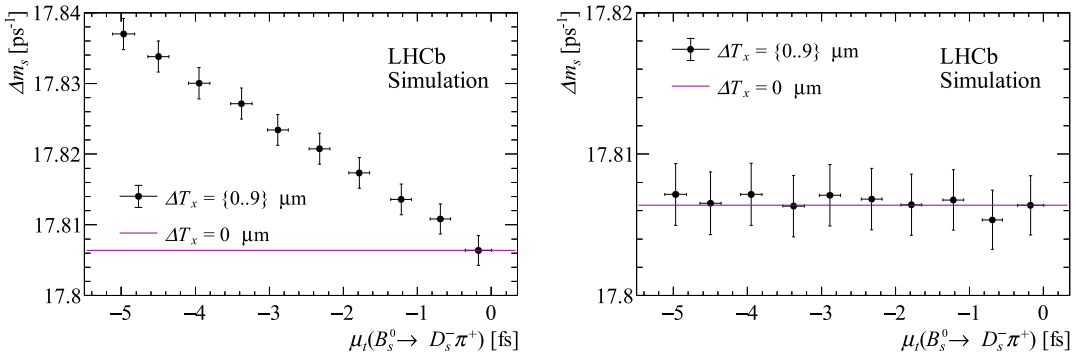

Figure 12: Value of Δm_s versus the decay-time bias μ_t obtained from misaligned simulated signal samples. The left figure has no correction applied to the reconstructed lifetimes and shows a decreasing value of Δm_s with the bias. The right figure shows that by applying a correction for the average bias on the reconstructed decay times, the fitted value of Δm_s is unbiased for different misalignment values.

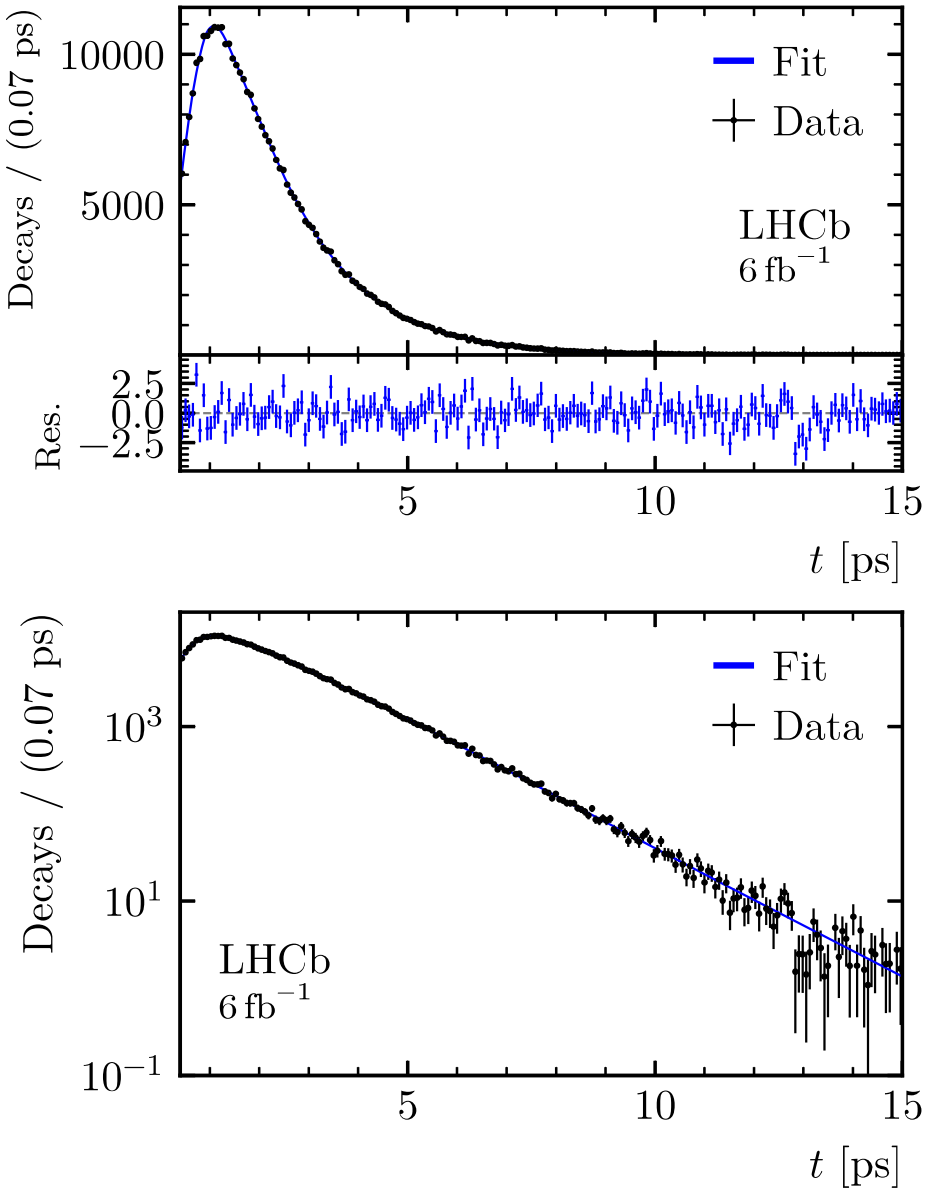

Figure 13: Decay-time distribution of the combined data set in linear (top) and logarithmic scale (bottom). The blue line corresponds to the fit. The top plot also shows the residual (Res.) of the data points with respect to the fit, normalized to the uncertainty of the data points.